Hyper-Hue and EMAP on Hyperspectral Images for Supervised Layer Decomposition of Old Master Drawings

AmirAbbas Davari*, Nikolaos Sakaltras*, Armin Haeberle[†], Sulaiman Vesal*, Vincent Christlein*
Andreas Maier* and Christian Riess*
*Pattern Recognition Lab, Department of Computer Science, Friedrich-Alexander University
Erlangen Nuernberg, Erlangen, Germany, Email: amir.davari@fau.de
[†]Bibliotheca Hertziana - Max-Planck-Institute for Art History, Rome, Italy

Abstract—Old master drawings were mostly created step by step in several layers using different materials. To art historians and restorers, examination of these layers brings various insights into the artistic work process and helps to answer questions about the object, its attribution and its authenticity. However, these layers typically overlap and are oftentimes difficult to differentiate with the unaided eye. For example, a common layer combination is red chalk under ink.

In this work, we propose an image processing pipeline that operates on hyperspectral images to separate such layers. In particular, we propose to use two descriptors in hyperspectral historical document analysis, namely hyper-hue and extended multi-attribute profile (EMAP). We show that hyperspectral images enable better layer separation than RGB images, and that spectral focus stacking is an important preprocessing step towards that goal. Our comparative results with other features underline the efficacy of the three proposed improvements.

Keywords-Old Master Drawing, Layer Separation, Hyper-Hue, EMAP, Spectral Focus Stacking

I. INTRODUCTION

Red chalk was a highly popular drawing material until the late nineteenth century [1], [2]. In the artistic work process, it has oftentimes been used for creating a first sketch, in order to later overdraw it with ink. For art historians today, these sketches provide insights into the creation process of the art work. In particular, differences between the underlying sketch and the drawing above can indicate changes in the direction of the work.

For separating the layers of ink and strokes of chalk on a drawing, current state of the art consists of destructive and non-destructive methods. Conservators and museums are oftentimes understandably hesitant to apply destructive approaches to old master drawings. Image analysis techniques are typically non-destructive, for example the classification of brush strokes [3]. To our knowledge, only few works perform layer separation of the old drawings. One study separates brush strokes on van Gogh's "Self portrait with grey felt hat" via RGB image processing [4]. However, this method has to rely on a good separation of all strokes in RGB domain.

In this work, we investigate the particular case where red chalk is overdrawn by ink. A widely used technique to visualize structures below a layer of ink is to image via infrared reflectography (IRR) the object in the infrared range, at wavelengths above 2000 nm. In this regime, ink becomes transparent. However, this approach is not applicable to make red chalk visible: red chalk consists primarily of natural red clay containing iron oxide, and the reflectance of red chalk at wavelengths above 2000 nm is very similar to the image carrier (i.e., the paper or parchment). As a consequence, this range of wavelengths can not be used to visualize over-painted strata of red chalk [5], [6]. The difficulties of displaying and distinguishing the drawn strata by conventional IRR, or with remission-spectroscopy poses a significant challenge to recover the underlying substrate layers. This is also shown in the comparative sequence of images from the apocryphal Rembrandt drawings in Munich (visible spectrum versus infrared imaging), published by Burmester and Renger [5].

In this work, we propose to close this diagnostic gap to visualize red chalk below ink by using hyperspectral imaging together with a pattern recognition pipeline. There are many works in the literature that used hyperspectral imaging for document analysis and proved its superiority to RGB imaging [7], [8], [9]. Our contributions are three-fold: We propose two descriptors for using in hyperspectral historical document analysis, namely hyper-hue and extended multi-attribute profile (EMAP), and we address a common artifact in hyperspectral imaging called focus shifting, and propose spectral focus stacking as its solution. We evaluate the proposed approaches on drawings that are created to exactly mimic the original work process.

II. HYPERSPECTRAL DESCRIPTORS FOR SKETCH LAYER SEPARATION

A. Extended Multi-Attribute Profile (EMAP)

Attribute profiles are popular tools in remote sensing [10], [11]. The idea is to abstract morphological operators like opening or closing from specific shapes of structuring elements. The building blocks of attribute profiles are attribute filters that operate on connected components (CC) of lower or equal gray level intensities. On each CC in the image, an attribute A (e.g., the area, standard deviation, or diameter of the CC) is computed and compared to a threshold λ. If $A(CC_i) \geq \lambda$, it is preserved. Otherwise, the i-th CC is merged with the closest neighboring CC. Analogously to classical morphological operators, attribute thickening (denoted as $\Phi_\lambda^A(f)$) is the process of merging the CCs of image f to neighboring CC with higher gray level. Attribute thinning (denoted as $\gamma_\lambda^A(f)$) is the process of merging the CCs of image f to neighboring CC with lower gray level.

The attribute thinning profile of an image f, denoted by $\Pi(\gamma_\lambda^A)(f)$, is generated by concatenating series of attribute thinning with an increasing criterion size λ:

$$\Pi(\gamma_\lambda^A)(f) = \{\Pi(\gamma_\lambda^A) : \Pi(\gamma_\lambda^A) = \gamma_\lambda^A(f), \forall \lambda \in [0, ..., n]\} \quad (1)$$

Analogously, attribute thickening profile of an image f, denoted by $\Pi(\Phi_\lambda^A)(f)$, is generated by concatenating series of attribute thickenings with an increasing criterion size λ:

$$\Pi(\Phi_\lambda^A)(f) = \{\Pi(\Phi_\lambda^A) : \Pi(\Phi_\lambda^A) = \Phi_\lambda^A(f), \forall \lambda \in [0, ..., n]\} \quad (2)$$

The attribute profile (AP) is generated by concatenating series of attribute thickening and thinning profiles with an increasing criterion size λ:

$$AP(f) = \{ \overset{\forall \lambda \in [\lambda_1, ..., \lambda_n]}{\Pi(\gamma_\lambda^A)(f)}, f, \overset{\forall \lambda \in [\lambda_1, ..., \lambda_n]}{\Pi(\Phi_\lambda^A)(f)} \} \quad (3)$$

In the case of $\lambda = 0$, $\Pi(\gamma_0^T) = \Pi(\Phi_0^T) = f$. Therefore, attribute profile vector's size will be $2n + 1$, i.e., n for attribute thinning, n for attribute closing and one for the original image.

By using more than one attribute and concatenating the generated APs, multi-attribute profiles (MAPs) are generated. Finally, stacking the computed MAPs over each spectral channel of a multi-/hyper-spectral image results in the extended multi-attribute profile (EMAP). EMAPs use both spatial and spectral signatures of a hyperspectral image (HSI) and are capable of modeling and describing an image based on different attributes, e.g. area, standard deviation and moment of the CCs. In this work, we used the same attributes and threshold values as the work by Ghamisi et al. [12].

B. Hyper-Hue

Let $(0, \ldots, 0)^T$ denote the black in n dimensions, which we call HyperBlack, and let analogously denote $(1, \ldots, 1)^T$ HyperWhite. Let furthermore $\mathbf{a}$ denote the achromatic hyper-axis, which is the normal vector of the hyper-chromatic plane $\mathbf{P}$ that contains the point HyperBlack. In order to mathematically define $\mathbf{P}$, we derive its spanning unit vectors. In an n-dimensional space, $\mathbf{P}$ is spanned by $n-1$ pairwise perpendicular n-dimensional unit vectors, $\{\mathbf{u}_1, \mathbf{u}_2, \ldots, \mathbf{u}_n\}^T$. The vectors $\mathbf{u}_i$ have the properties that (1) they start from the point HyperBlack, (2) they are pairwise perpendicular, (3) they are unit vectors and therefore their norm is 1, (4) the direction of $\mathbf{u}_1$ points towards the projection of $(1, \ldots, 0)^T$ on the plane $\mathbf{P}$, (5) $\mathbf{u}_i$ are orthogonal to $\mathbf{a}$.

Suppose the first $n-m$ elements of $\mathbf{u}_i$ are 0 and the remaining m elements are non-zero. From these m elements, denote the first one as a and the remaining elements as b. As it is derived in [13], we obtain a basis for $\mathbf{P}$ by setting $a = \frac{m-1}{\sqrt{m(m-1)}}$ and $b = \frac{-1}{\sqrt{m(m-1)}}$. The projection of a hyperspectral point $\mathbf{x}_j$ onto $\mathbf{P}$ is then

$$\mathbf{c}_j = (\mathbf{x}_j \cdot \mathbf{u}_1)\mathbf{u}_1 + (\mathbf{x}_j \cdot \mathbf{u}_2)\mathbf{u}_2 + \cdots + (\mathbf{x}_j \cdot \mathbf{u}_n)\mathbf{u}_n \ . \quad (4)$$

Liu et al. [13] defined hyper-hue $\mathbf{h}$, saturation S and intensity I of a hyperspectral point $\mathbf{x}$ via its projection $\mathbf{c}$ as

$$\mathbf{h} = \frac{\mathbf{c}}{\|\mathbf{c}\|} \ , \quad (5)$$

$$S = \frac{\|\mathbf{c}\|}{c_{\max}} = \max\{x_1, \ldots, x_n\} - \min\{x_1, \ldots, x_n\} \ , \quad (6)$$

$$I = \frac{1}{n}(x_1 + \cdots + x_n) \ . \quad (7)$$

In this way, an extension of HSI color space is defined for hyperspectral images.

III. PROCESSING PIPELINE

A. Sensitivity Normalization

Hyperspectral imaging setups suffer from various limitations and artifacts which need to be corrected. The sensitivity of an HS camera sensor along the spectrum is not uniform. Using a white reference, the uneven sensitivity can be corrected. Fig. 1-(a) shows the sensitivity diagram of the sensor measured from a white reference. The inverse of this diagram is used as the sensitivity normalization coefficient. Fig. 1 (b)-(c) show the sensitivity-normalized version of the channel 20 (representing 407.31 nm wavelength) and channel 230 (representing 932.82 nm wavelength), respectively.

Every imaging setup needs good lighting for an acceptable acquisition and HS imaging is not an exception. In real world
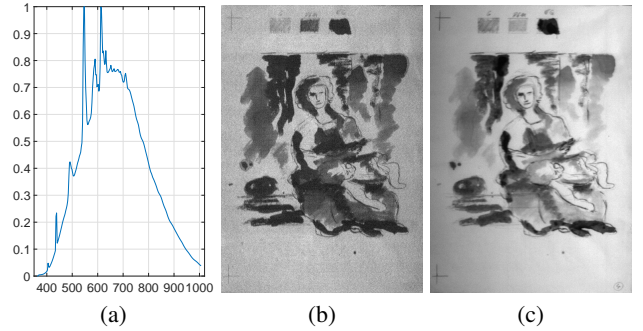

Figure 1: Sensitivity-normalized sample channels of the raw hyperspectral image. (a) Normalized hyperspectral sensor sensitivity vs. wavelength (nm), (b) channel 20, (c) channel 230.
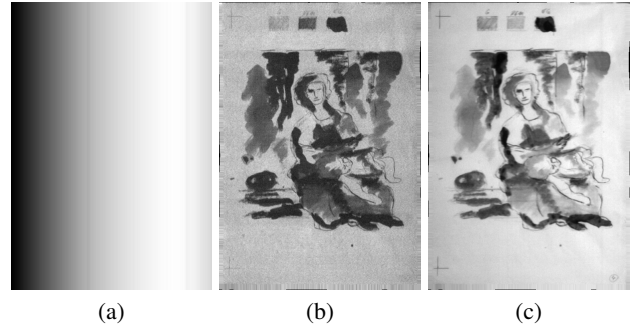

Figure 2: Illumination-corrected and registered sample channels of the raw hyperspectral image to the ground truth. (a) Normalized uneven illumination field, (b) channel 20, (c) channel 230.

scenario, in a museum for instance, the subject may not be evenly illuminated. To simulate this situation, we sidelit our scene. Using a white reference, we estimate the uneven lighting, as shown in Fig. 2-(a). Fig. 2 (b)-(c) show the illumination-corrected version of the Fig. 1 (b)-(c), respectively.

B. Focus Stacking

Common HS cameras suffer from focus shifting, which is a well-known artifact in the field [14]. It leads to the issue that not all of the channels are simultaneously in focus when making a multispectral acquisition. Fig. 3 shows this behavior for two hyperspectral images, namely H_1 and H_2. For acquiring H_1, the lens is focused with the blue range aimed to be in focus. H_2, on the other hand, is captured by having the red spectrum in focus. Fig. 3 (a) shows channel 41, representing 458.82 nm wavelength, of H_1. Fig. 3 (b) shows the same channel of H_2. Especially on fine edges, we can observe that (a) is sharper and more in focus. Similarly, Fig. 3 (c) and (d) show the channel 200, representing the 854.97 nm wavelength, of H_1 and H_2, respectively. This time the channel corresponding to H_2 is sharper than H_1.

One contribution of this work lies in producing one hyperspectral image with all channels in focus via spectral focus stacking. To this end, we acquire two images with two different focus points, one in the blue spectrum and one in the red spectrum. The final all-in-focus image is generated from the in-focus channels of the two input images. In our work, we generate our final all-in-focus image by using the first 75 channels from H_1 and the remaining 183 channels from H_2. We quantitatively compared our all-in-focus HSI with H_1 and H_2.

(a)   (b)   (c)   (d)

Figure 3: H_1 which is focused on the blue spectrum vs. H_2 which is focused on the red spectrum. (a) H_1 channel 41 (457.82 nm), (b) H_2 channel 41 (457.82 nm), (c) H_1 channel 200 (854.97 nm), (d) H_2 channel 200 (854.97 nm).

C. Classification

We assume that it is feasible to obtain a limited number of labeled pixels by a specialist, for example an art historian. This allows to use supervised learning for the layer separation. We consider the three classes red chalk, diluted red chalk and black ink. Classification is performed using a random forest (RF), with 10 trees. The number of variables for training the trees and bagging is set to the square root of the number of features [15]. We used 100 random samples per class for training and the rest for testing. We repeated this process 25 times and reported the average classification performance metrics and their standard deviation (SD). In our dataset, the number of pixels for these classes is 10791, 23528 and 85000, respectively. For training, we selected 100 pixels from each class, which corresponds to 0.9%, 0.4% and 0.1% of each class, respectively.

IV. EVALUATION

A. Dataset

1) Phantom Data: We created a set of sketches with multiple layers of graphite, chalk, and different inks of the same chemical composition that were commonly used in old master drawings. After each layer was drawn, the picture was scanned with a book scanner (Zeutschel OS 12000, in RGB mode). This step-by-step documentation of the controlled creation process allows to compute ground truth drawing layers, by subtracting two subsequent scanned images. A sample sketch from this data is shown in Figure 4.

2) Hyperspectral Imaging: We use a Specim PFD-CL-65-V10E hyperspectral camera equipped with a CMOS sensor, capable of capturing the spectrum between 400 nm to 1000 nm. We use a lens with 16 mm focal length. The distance between the subject and the camera is 68 cm. The document is illuminated with a 500 W tungsten lamp.

3) Simulated RGB: Historic documents are highly sensitive to light exposure. Thus, it is important to compare different imaging modalities at identical dose levels. To achieve this, we synthesize an RGB image from the HSI image by channel averaging, which ensures that both images have the same exposure. The blue, green, and red colors in RGB domain corresponds to wavelengths between 415 nm and 495 nm (HSI channels 24 to 56), 495 nm to 570 nm (HSI channels 57 to 87) and 620 nm to 750 nm (HSI channels 108 to 156), respectively. We generated the red, green and blue channels by taking the average of HSI channels 108-156, 57-87 and 24-56, respectively. Figure 5 shows the simulated RGBs from the HSIs, before and after pre-processing.
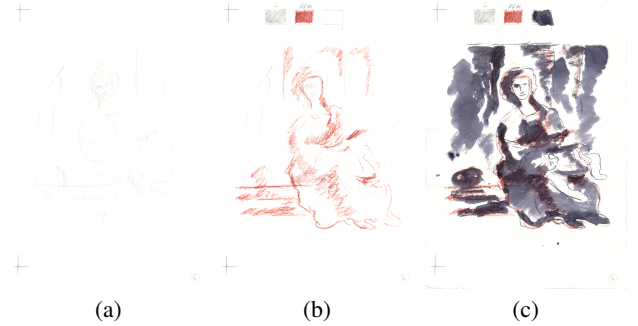

(a)   (b)   (c)

Figure 4: Sample layers from the data of the creation process as basis of evaluation: (a) Step 1: first graphite sketch. (b) Step 2: underdrawings with red chalk. (c) Steps 3 and 4: drawing with pen and iron gall ink plus final wash with two dilutions of ink in "two bowl technique", as described by Armenini [16][pp.54-55]. and Meder [17][pp.54-55]. Delineation after: Stefano della Bella, "Mother with two children", Florence, Galleria degli Uffici, Gabinetto Disegni e stampe, Inv.-Nr. 5937S.
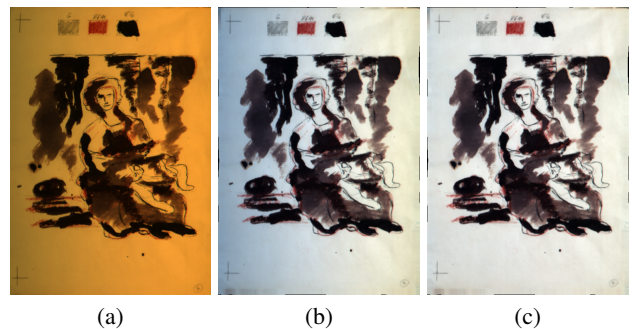

(a)   (b)   (c)

Figure 5: Simulated RGB image from the hyperspectral image. (a) RGB image generated from the raw HSI, (b) RGB image generated from the sensitivity-normalized HSI in Fig. 1, (c) RGB image generated from illumination-corrected HSI in Fig. 2.

B. Evaluation Protocol

1) Registration of HSI to the ground truth: Our ground truth, generated from Fig. 4, is acquired by a board scanner. The HSI images are acquired via a line scanner hyperspectral camera. Different modalities, resolutions, aspect ratios and the non-flat surface of the paper make the images from these modalities geometrically different. In order to compare the HSI analysis output, hyperspectral images need to be registered to the board scanner image. We use residual complexity similarity measure (RC) [18] to register the HSI to the RGB image acquired by the board scanner, which showed good results in a previous study [19].

2) Metrics: To evaluate the classification performances, we used overall accuracy (OA), average accuracy (AA) and Kappa coefficient metrics. OA is the number of correctly classified instances divided by the number of all samples, while AA is the mean class-based accuracies. The Kappa statistic is a measure of how closely the classified samples matches the ground truth. By measuring the expected accuracy, it results in a statistic expressing the accuracy of a random classifier.

C. Results

1) Impact of Spectral Focus Stacking: In order to study the effect of spectral focus stacking, we conducted two sets of

Table I: Spectral focus stacking results.

Feature	AA% ($\pm$SD)	OA% ($\pm$SD)	Kappa ($\pm$SD)
Simulated RGB image from HSI			
H_1	70.63 ($\pm$1.41)	60.82 ($\pm$2.51)	0.3515 ($\pm$0.0227)
H_2	72.32 ($\pm$1.15)	63.62 ($\pm$3.09)	0.3777 ($\pm$0.0313)
Focus Stacking	**73.72** ($\pm$1.10)	**64.96** ($\pm$2.40)	**0.3980** ($\pm$0.0257)
Illumination-corrected HSI			
H_1	74.76 ($\pm$0.94)	64.67 ($\pm$1.45)	0.3998 ($\pm$0.0169)
H_2	76.12 ($\pm$0.96)	66.34 ($\pm$1.42)	0.4186 ($\pm$0.0165)
Focus Stacking	**76.57** ($\pm$0.94)	**67.21** ($\pm$3.56)	**0.4304** ($\pm$0.0366)

Table II: Performances of the features.

Feature	AA% ($\pm$SD)	OA% ($\pm$SD)	Kappa ($\pm$SD)
SimRGB	71.83 ($\pm$0.79)	62.05 ($\pm$1.90)	0.3632 ($\pm$0.0178)
SimRGB-IC	73.72 ($\pm$1.10)	64.96 ($\pm$2.40)	0.3980 ($\pm$0.0257)
SimRGB-IC-SI	74.29 ($\pm$0.61)	66.08 ($\pm$2.57)	0.4119 ($\pm$0.0261)
SimRGB-IC-EMAP	74.63 ($\pm$0.77)	67.25 ($\pm$1.84)	0.4251 ($\pm$0.0170)
HSI	75.43 ($\pm$1.05)	66.94 ($\pm$2.11)	0.4196 ($\pm$0.0217)
HSI-IC	76.57 ($\pm$0.94)	67.21 ($\pm$3.56)	0.4304 ($\pm$0.0366)
HSI-DR	80.35 ($\pm$0.66)	72.58 ($\pm$1.53)	0.5019 ($\pm$0.0183)
HSI-h	**83.00** ($\pm$0.47)	**77.39** ($\pm$1.28)	**0.5731** ($\pm$0.0161)
HSIhSI	82.86 ($\pm$0.52)	77.16 ($\pm$1.53)	0.5701 ($\pm$0.0213)
HSIhSI-DR	79.58 ($\pm$0.86)	71.00 ($\pm$2.41)	0.4817 ($\pm$0.0273)
HSI-EMAP	**82.61** ($\pm$1.11)	**77.35** ($\pm$2.53)	**0.5719** ($\pm$0.0350)
HSIhSI-EMAP	**83.08** ($\pm$0.89)	**77.70** ($\pm$1.18)	**0.5766** ($\pm$0.0191)

experiments on simulated RGB images and HS images. In the first experiment, we generated RGB images from H_1, H_2 and all-in-focus HSI. In the second experiment, we carried out the classification on the illumination-corrected H_1, H_2 and all-in-focus HSI. The results for these two experiments are presented in Table I. It can be seen that in both scenarios, spectral focus stacking yields better AA, OA and Kappa performance.

2) Layer Separation Performance of the Proposed Features: As spectral focus stacking results in better performance, the remaining computations are performed over all-in-focus images. To study the impact of illumination correction, hyper-hue, and EMAP, we generated the following features.

- SimRGB: Simulated RGB image, generated from the illumination-uncorrected all-in-focus HSI,
- SimRGB-IC: Simulated RGB image, generated from the illumination-corrected HSI,
- SimRGB-IC-SI: SimRGB-IC, saturation (S in Eq. 6) and intensity (I in Eq. 7) concatenated together,
- SimRGB-IC-EMAP: EMAP computed on SimRGB-IC. We used area as the only EMAP attribute with 20 thresholds λ, selected by following Ghamisi *et al.* [12],
- HSI: Illumination-uncorrected all-in-focus HSI,
- HSI-IC: Illumination-corrected all-in-focus HSI,
- HSI-DR: HSI-IC projected to its PCA components such that 99.9% of its variance are preserved,
- HSI-h: Hyper-hue computed from the illumination-corrected HSI,
- HSIhSI: HSI-IC, hyper-hue, saturation (S) and intensity (I) concatenated together,
- HSIhSI-DR: Dimensionality reduced HSIhSI via PCA so that 99.9% of its variance is preserved.
- HSI-EMAP: EMAP computed on dimensionality reduced HSI-IC. EMAP's parameters are chosen analogously to SimRGB-IC-EMAP,
- HSIhSI-EMAP: EMAP computed on dimensionality reduced HSIhSI. EMAP parameters are chosen analogously to SimRGB-IC-EMAP.

Quantitative results are shown in Tab. II. Illumination correction always improves the results, both for SimRGB vs. SimRGB-IC and for HSI vs. HSI-IC. Furthermore, the comparing HSI-IC with SimRGB-IC shows the advantage of hyperspectral images over RGB. The PCA in HSI-DR, further improves the HSI performance. However, in hyperspectral remote sensing, it has been shown that dimensionality reduction alone is outperformed by problem-specific descriptors. We observe a similar behavior here, as hyper-hue computed over HSI (HSI-h) results in a big jump in performance. Furthermore, the standard deviation of HSI-h is smallest among all features, which indicates a high stability. Neither combining hyper-hue, saturation and intensity on the HSI image (HSI-hSI), nor an additional dimensionality reduction (HSI-hSI-DR) exceed the performance of hyper-hue alone. HSI-EMAP results in a similar performance as HSI-h.
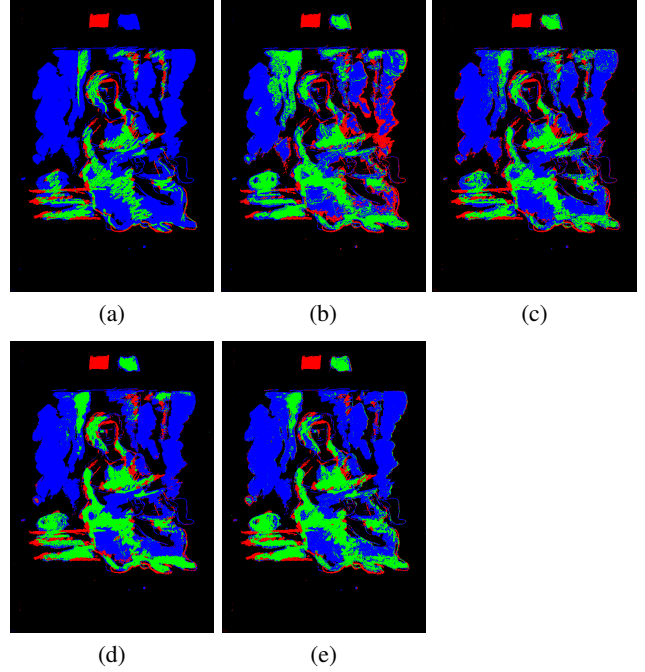

Figure 6: Label maps. (a) Ground truth, (b) SimRGB, (c) HSI-h, (d) HSI-EMAP, (e) HSIhSI-EMAP.

Finally, HSIhSI-EMAP best separates the layers.

Qualitative results are shown in Fig. 6. Fig. 6 (a) represents the ground truth (GT), where red denotes red chalk, green denotes red chalk overlaid by black ink, and blue color denotes black ink. Black denotes the background and is ignored during classification. As it can be observed from this image, SimRGB shows many misclassifications, which is highly improved by HSI-h, HSI-EMAP and HSIhSI-EMAP.

V. CONCLUSION AND DISCUSSION

In this work, we proposed and evaluated a hyperspectral imaging pipeline for decomposing the layers of old Master drawings. Our particular focus was on distinguishing the commonly used red chalk and black ink. We propose two descriptors to the field of hyperspectral historical document analysis, namely hyper-hue and extended multi-attribute profile. We also address focus shifting, an artifact in hyperspectral imaging, by focus stacking.

Our comparative results confirm that hyperspectral images are, at identical resolution and SNR, more informative than RGB images and result in better layer separation performance. EMAP and hyper-hue both outperform the raw hyperspectral features, and focus stacking of hyperspectral images positively impacts the layer separation.

REFERENCES

[1] T. Brachert, *Lexikon historischer Maltechniken: Quellen, Handwerk, Technologie, Alchemie.* Callwey, 2001.

[2] N. Eastaugh, V. Walsh, T. Chaplin, and R. Siddall, *Pigment compendium: a dictionary of historical pigments.* Routledge, 2007.

[3] J. Li, L. Yao, E. Hendriks, and J. Z. Wang, "Rhythmic Brushstrokes Distinguish van Gogh from His Contemporaries: Findings via Automated Brushstroke Extraction," *IEEE Transactions on Pattern Analysis and Machine Intelligence*, vol. 34, no. 6, pp. 1159–1176, 2012.

[4] M. Shahram, D. G. Stork, and D. Donoho, "Recovering layers of brush strokes through statistical analysis of color and shape: an application to van Gogh's self portrait with grey felt hat," in *Computer image analysis in the study of art*, vol. 6810. International Society for Optics and Photonics, 2008, p. 68100D.

[5] A. Burmester and K. Renger, "Neue Ansätze zur technischen Erforschung von Handzeichnungen: Untersuchungen der Münchner Rembrandt-Fälschungen im Nahen Infrarot," *Maltechnik Restauro*, vol. 92, no. 3, pp. 9–34, 1986.

[6] F. Mairinger, *Strahlenuntersuchung an Kunstwerken.* EA Seemann Verlag2, 2003.

[7] A. Pelagotti, A. Del Mastio, A. De Rosa, and A. Piva, "Multispectral imaging of paintings," *IEEE Signal Processing Magazine*, vol. 25, no. 4, 2008.

[8] M. Lettner, F. Kleber, R. Sablatnig, and H. Miklas, "Contrast enhancement in multispectral images by emphasizing text regions," in *Document Analysis Systems, 2008. DAS'08. The Eighth IAPR International Workshop on*. IEEE, 2008, pp. 225–232.

[9] M. Diem, M. Lettner, and R. Sablatnig, "Multi-Spectral Image Acquisition and Registration of Ancient Manuscripts," in *Performance Evaluation for Computer Vision 31st AAPR/OAGM Workshop 2007*, 2007, pp. 129–136.

[10] E. J. Breen and R. Jones, "Attribute openings, thinnings, and granulometries," *Computer Vision and Image Understanding*, vol. 64, no. 3, pp. 377–389, 1996.

[11] M. Dalla Mura, J. A. Benediktsson, B. Waske, and L. Bruzzone, "Morphological attribute profiles for the analysis of very high resolution images," *Geoscience and Remote Sensing, IEEE Transactions on*, vol. 48, no. 10, pp. 3747–3762, 2010.

[12] P. Ghamisi, J. A. Benediktsson, G. Cavallaro, and A. Plaza, "Automatic framework for spectral–spatial classification based on supervised feature extraction and morphological attribute profiles," *IEEE Journal of Selected Topics in Applied Earth Observations and Remote Sensing*, vol. 7, no. 6, pp. 2147–2160, 2014.

[13] H. Liu, S.-H. Lee, and J. S. Chahl, "Transformation of a high-dimensional color space for material classification," *JOSA A*, vol. 34, no. 4, pp. 523–532, 2017.

[14] M. E. Klein, B. J. Aalderink, R. Padoan, G. De Bruin, and T. A. Steemers, "Quantitative hyperspectral reflectance imaging," *Sensors*, vol. 8, no. 9, pp. 5576–5618, 2008.

[15] L. Breiman, "Random forests," *Machine Learning*, vol. 45, pp. 5–32, 2001.

[16] G. ARMENINI, *De'veri precetti della pittura ... libri tre, etc*. F. Tebaldini, 1586. [Online]. Available: https://books.google.co.uk/books?id=7b1lAAAAcAAJ

[17] J. Meder, *Die Handzeichnung: ihre Technik und Entwicklung.* A. Schroll, 1919, no. 738.

[18] A. Myronenko and X. Song, "Intensity-based image registration by minimizing residual complexity," *IEEE Transactions on Medical Imaging*, vol. 29, no. 11, pp. 1882–1891, 2010.

[19] A. Davari, T. Lindenberger, A. Häberle, V. Christlein, A. Maier, and C. Riess, "Image Registration for the Alignment of Digitized Historical Documents," *ArXiv e-prints*, Dec. 2017.